

Surface-state-dominated transport in crystals of the topological crystalline insulator In-doped $\text{Pb}_{1-x}\text{Sn}_x\text{Te}$

Ruidan Zhong,^{1,2,*} Xugang He,^{1,3} J. A. Schneeloch,^{1,3} Cheng Zhang,^{1,2} Tiansheng Liu,^{1,4} I. Pletikosić,^{1,5} T. Yilmaz,⁶ B. Sinkovic,⁶ Qiang Li,¹ Wei Ku,¹ T. Valla,¹ J. M. Tranquada,^{1,†} and Genda Gu¹

¹Condensed Matter Physics and Materials Science Department, Brookhaven National Laboratory, Upton, New York 11973, USA

²Materials Science and Engineering Department, Stony Brook University, Stony Brook, New York 11794, USA

³Department of Physics and Astronomy, Stony Brook University, Stony Brook, New York 11794, USA

⁴School of Chemical Engineering and Environment, North University of China, Shanxi 030051, China

⁵Department of Physics, Princeton University, Princeton, New Jersey 08544, USA

⁶Department of Physics, University of Connecticut, Storrs, Connecticut 06269, USA

(Received 6 February 2015; revised manuscript received 15 April 2015; published 29 May 2015)

Three-dimensional topological insulators and topological crystalline insulators represent new quantum states of matter, which are predicted to have insulating bulk states and spin-momentum-locked gapless surface states. Experimentally, it has proven difficult to achieve the high bulk resistivity that would allow surface states to dominate the transport properties over a substantial temperature range. Here we report a series of indium-doped $\text{Pb}_{1-x}\text{Sn}_x\text{Te}$ compounds that manifest huge bulk resistivities together with evidence consistent with the topological character of the surface states for $x \gtrsim 0.35$, based on thickness-dependent transport studies and magnetoresistance measurements. For these bulk-insulating materials, the surface states determine the resistivity for temperatures beyond 20 K.

DOI: [10.1103/PhysRevB.91.195321](https://doi.org/10.1103/PhysRevB.91.195321)

PACS number(s): 72.20.-i, 73.20.At

I. INTRODUCTION

A great deal of interest has been generated by the theoretical prediction and experimental realization of three-dimensional (3D) topological insulator (TI) materials [1,2]. In certain semiconductors with strong spin-orbit coupling effects, the chiral character of metallic surface states is protected by time-reversal symmetry. A variety of 3D TI materials have been synthesized over the last few years [3], and the existence of the topologically protected surface states has been experimentally confirmed [1]; however, none of these materials have exhibited truly insulating bulk character.

Topological crystalline insulators (TCIs) are closely related to TIs, with the exotic surface states protected by crystal symmetries, rather than by time-reversal symmetry [4]. There has been considerable excitement since the first example, SnTe , was theoretically predicted [5] to exhibit topological surface states on {001}, {110}, and {111} surfaces of the rock-salt crystal structure, with quick experimental confirmation of the first case [6]. Soon after this discovery, the topological surface states in the alloys $\text{Pb}_{1-x}\text{Sn}_x\text{Se}$ and $\text{Pb}_{1-x}\text{Sn}_x\text{Te}$ were verified by angle-resolved photoemission spectroscopy (ARPES) [7–9], thus expanding the range of relevant materials.

For applications in spintronics, it is important to have the resistivity dominated by the topologically protected surface states. Substantial efforts have been made on the TI material Bi_2Se_3 and its alloys to reduce the bulk carrier density; however, while it has been possible to detect the signature of surface states in the magnetic-field dependence of the resistivity at low temperature [10–12], attempts to compensate intrinsic defects [13,14] have not been able to raise the bulk resistivity above 15 Ω cm. Theoretical analysis suggests that

even with perfect compensation of donor and acceptor defects, the resulting random Coulomb potential limits the achievable bulk resistivity [15].

The solid solution $\text{Pb}_{1-x}\text{Sn}_x\text{Te}$ provides a fresh opportunity for exploration. Figure 1(b) illustrates the expectations for this system. With a small amount of In doping, the band gap should be at the Fermi level, E_F , for x in the range of 0.25–0.3 [16]. The topological character changes from nontrivial at $x = 1$ to trivial at $x = 0$, with a topological quantum phase transition at $x_c \approx 0.35$, corresponding to the point at which band inversion begins [8,17–19]. In our previous investigation of indium-induced superconductivity in $\text{Pb}_{0.5}\text{Sn}_{0.5}\text{Te}$ single crystals [20], we observed a nonmonotonic variation in the normal-state resistivity with indium concentration, with a maximum at 6% indium doping. Further motivation has come from older work [21] on various compositions of $(\text{Pb}_{1-x}\text{Sn}_x)_{1-y}\text{In}_y\text{Te}$. (Note that In doping reduces the lattice parameter [20], so that, like pressure [16], it should reduce x_c for band inversion.) Hence, we have performed a systematic study, growing and characterizing single crystals with six Pb/Sn ratios ($x = 0.2, 0.25, 0.3, 0.35, 0.4, 0.5$) and a variety of In concentrations ($y = 0–0.2$).

II. MATERIAL SYNTHESIS AND CHARACTERIZATION

Single crystal samples with nominal composition, $(\text{Pb}_{1-x}\text{Sn}_x)_{1-y}\text{In}_y\text{Te}$ ($x_{\text{nom}} = 0.2–0.5$, $y_{\text{nom}} = 0–0.2$), were prepared via the modified Bridgman method. Stoichiometric mixtures of high-purity (99.999%) elements were sealed in double-walled evacuated quartz ampoules. The ampoules were heated at 950°C in a box furnace and rocked to achieve good mixing of the ingredients. The crystal growth took place via slow cooling from 950 to 760°C in 1.5°C/hr, followed by gradual cooling to room temperature over another 3 days. Chemical composition values for x and y cited from here

*rzhong@bnl.gov

†jtran@bnl.gov

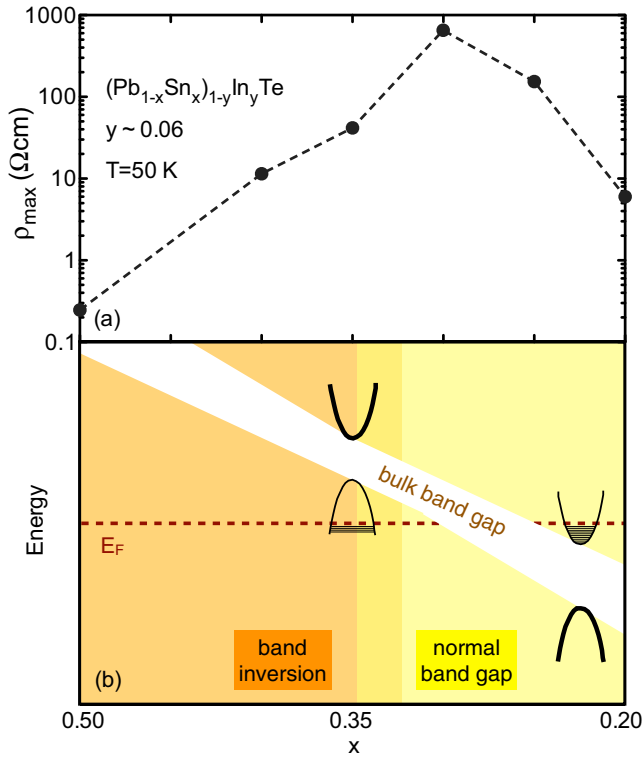


FIG. 1. (Color online) (a) Resistivity measured at 50 K for samples of $(\text{Pb}_{1-x}\text{Sn}_x)_{1-y}\text{In}_y\text{Te}$ for $y \sim 0.06$ as a function of x . (b) Schematic diagram of bulk electronic structure at low temperature as a function of x ; surface states are expected to be topologically nontrivial for $x \gtrsim 0.35$.

on correspond to the concentrations measured by energy-dispersive x-ray spectroscopy, with a measurement uncertainty of 2%.

III. ELECTRICAL RESISTIVITY

Nearly rectangular parallelepiped-shaped samples were prepared by polishing, with a typical geometry of 5 mm long, 1.5 mm wide, and 0.5 mm thick. Electrical resistance was measured in the standard four-probe configuration, using gold wires and silver paint for the ohmic contact on the top side, performed with a Keithley digital multimeter (Model 2001), where a Quantum Design (QD) Magnetic Property Measurement System was used for temperature control. Measurement errors due to the contact geometry were estimated to be less than 10%.

The measured resistivities, $\rho(T)$, for all samples, characterized by Sn concentration x and In concentration y , are summarized in Fig. 2. For each value of x , one can see that the resistivity of the parent compound ($y = 0$, black open triangles) reveals weakly metallic behavior; furthermore, the magnitudes of ρ in the In-free samples depend only modestly on x . With a minimum of $\sim 2\%$ indium doping, the low-temperature resistivity grows by several orders of magnitude, and the temperature dependence above $\sim 30\text{ K}$ exhibits the thermal activation of a semiconductor. The saturation of the resistivity for $T \lesssim 30\text{ K}$ is consistent with a crossover to surface-dominated conduction.

The maximum resistivities, surpassing $10^6\ \Omega\text{ cm}$, are observed for $x = 0.25\text{--}0.3$; the x dependence of resistivities at 50 K for $y \approx 0.06$ is summarized in Fig. 1(a). Even for $x = 0.35$, doping with 6% In results in a rise in resistivity of 6 orders of magnitude at 5 K; higher In concentrations tend to result in a gradual decrease in ρ . With increasing y , one eventually hits the solubility limit of In. Exceeding that point results in an InTe impurity phase, which is superconducting below 4 K and appears to explain the low-temperature drop in resistivity for $x = 0.4$ and $y = 0.16$ illustrated in Fig. 2(b).

Past studies [16,22] of various transport properties in $\text{Pb}_{1-x}\text{Sn}_x\text{Te}$ and the impact of In doping provide a basis for understanding the present results. For In concentrations of $\lesssim 0.06$, the In sites introduce localized states at a sharply defined energy that pins the chemical potential. In a small range of Sn concentration centered about $x = 0.25$, the chemical potential should be pinned within the band gap. Hence, the very large bulk resistivities observed for $x = 0.25$ and 0.3 are consistent with truly insulating bulk character.

IV. ARPES

To check the character of the electronic states near E_F , ARPES measurements were carried out on a Scienta SES-R4000 electron spectrometer at beamline U5UA at the former National Synchrotron Light Source (NSLS). The total instrumental energy resolution was $\sim 6\text{ meV}$; angular resolution was better than $\sim 0.15^\circ$. Thick ($2\text{--}5\ \mu\text{m}$) films of $(\text{Pb}_{0.7}\text{Sn}_{0.3})_{1-y}\text{In}_y\text{Te}$ were grown on freshly cleaved Bi_2Te_3 substrates [9], using the open hot-wall epitaxy method [23] and a single-source evaporator loaded with crushed single crystals of the desired composition. The substrate was kept at $\sim 300^\circ\text{C}$ during the growth. Composition of the films was checked by measuring photoemission from the shallow core levels (In $4d$, Sn $4d$, Te $4d$, and Pb $5d$) and comparing them with the source material.

Figure 3 shows the ARPES results for $x = 0.3$ with two different In concentrations. The valence band in Fig. 3(a) shows two overlapping states, split in k in the Rashba-like manner. This indicates that the surface states are already formed on surfaces of a material on the trivial side of the phase diagram ($x < 0.35$), and although they are expected to contribute to transport, they are not protected by any topological invariance. In that sense, they are very similar to the conventional Rashba surface states on Au(111). Increasing the In concentration to 16% in Fig. 3(b) clearly shifts the Fermi level towards the bulk conducting band, which seems to be just touching the Fermi level in the present case. Inside the bulk gap, the Rashba-like surface states can be seen on both the conduction side and the valence side, forming a conical like shape, but with a small gap still present between the two sides. This shows that at this composition, the material is very close to the critical point beyond which the cone should be complete (not gapped)—and topological surface states fully formed. A previous ARPES study has provided evidence for topological surface states at $x = 0.4$ (without In) [8].

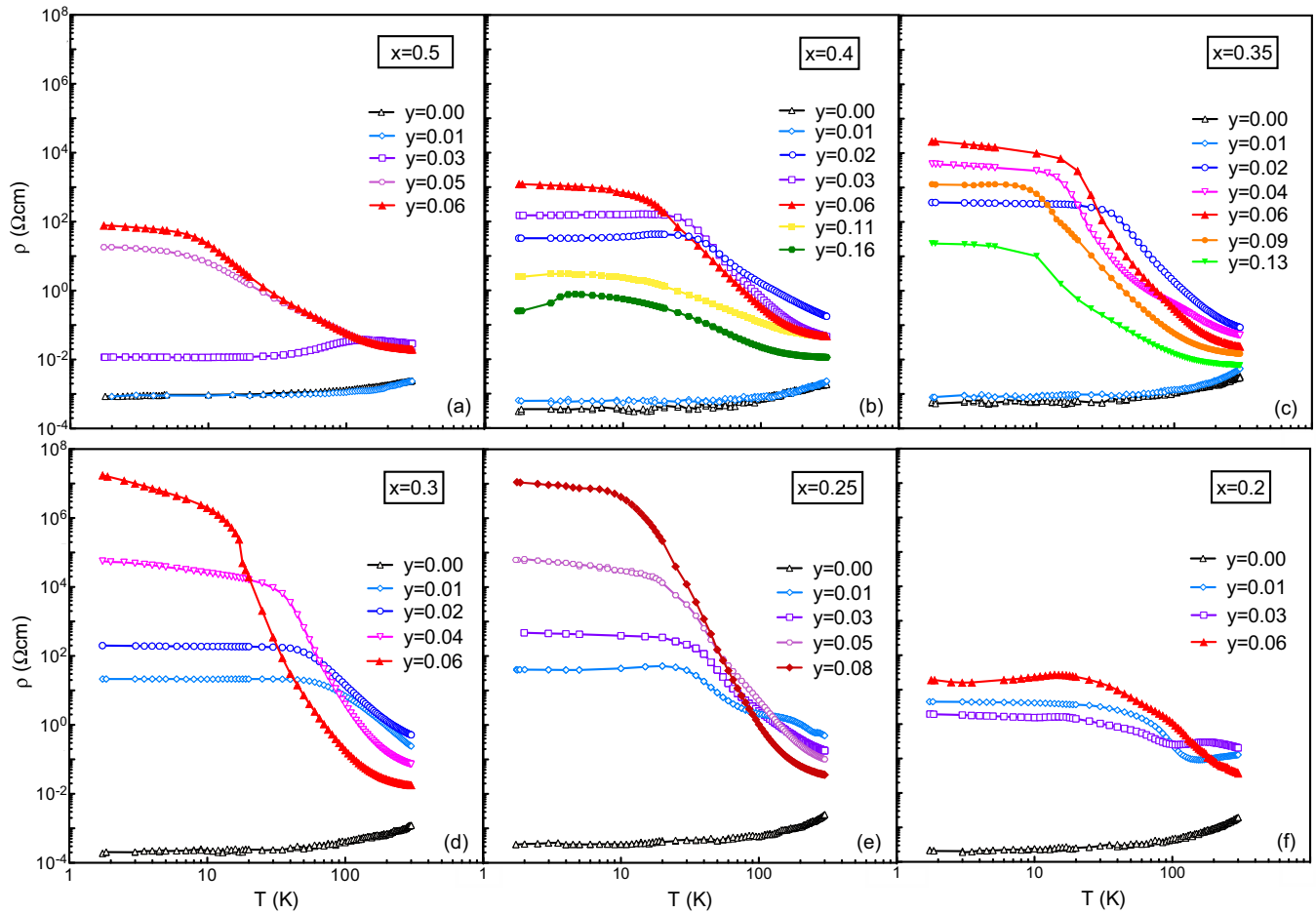


FIG. 2. (Color online) Temperature dependence of resistivity in $(\text{Pb}_{1-x}\text{Sn}_x)_{1-y}\text{In}_y\text{Te}$ for (a) $x = 0.5$, (b) $x = 0.4$, (c) $x = 0.35$, (d) $x = 0.3$, (e) $x = 0.25$, and (f) $x = 0.2$; the values of y are labeled separately in each panel. For each value of x , indium doping turns the metallic parent compound into an insulator, with low-temperature resistivity increasing by several orders of magnitude. The saturation of resistivity at temperatures below 30 K suggests that the surface conduction becomes dominant.

V. THICKNESS DEPENDENCE OF RESISTANCE

Now we concentrate on testing the character of the $x = 0.35$ and $y = 0.02$ sample, where we anticipate topological surface states. To test the contribution of the surface states to the

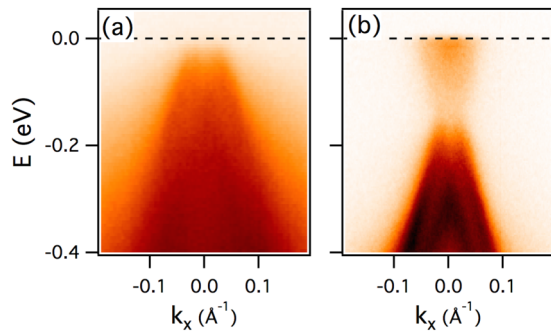


FIG. 3. (Color online) Electronic structure of (111) oriented films of $(\text{Pb}_{0.7}\text{Sn}_{0.3})_{1-y}\text{In}_y\text{Te}$. Dispersion of the valence band along the $\bar{K}-\bar{\Gamma}-\bar{K}$ line of the surface Brillouin zone (corresponding to the $W-L-W$ line of the bulk BZ), taken at ~ 20 K and at 17 eV photon energy for (a) $y = 0$ and (b) $y = 0.16$.

sample conductivity, we have measured the resistance $R(T)$ as a function of sample thickness [24–26]. The measurements involved sanding the bottom surface of the crystal with the top contacts remaining nominally constant. Following Syers *et al.* [26], in Fig. 4(a) we plot the ratio $r \equiv R(T)/R(300 \text{ K})$ for several thicknesses. Assuming parallel conduction channels for the surface and the bulk, with the bulk conduction being thermally activated, we fit $r(T)$ with

$$r(T)^{-1} = r_s^{-1} + r_b^{-1} e^{-\Delta/k_B T}, \quad (1)$$

where subscripts s and b label the surface and bulk contributions, respectively. The fitted results for r_s and r_b are plotted in Figs. 4(c) and 4(d); for the gap, we obtain $\Delta = 14.6 \pm 0.3$ meV. The parameter r_s , essentially the ratio of the bulk conductance at 300 K to the surface conductance, linearly extrapolates to zero in the limit of zero thickness. Alternatively, we can calculate the fraction of the conductivity in the surface channel, which is plotted in Fig. 4(b). Despite the fact that the sample thicknesses are quite large, we find that the surface states provide $>90\%$ of the conduction for $T < 20$ K.

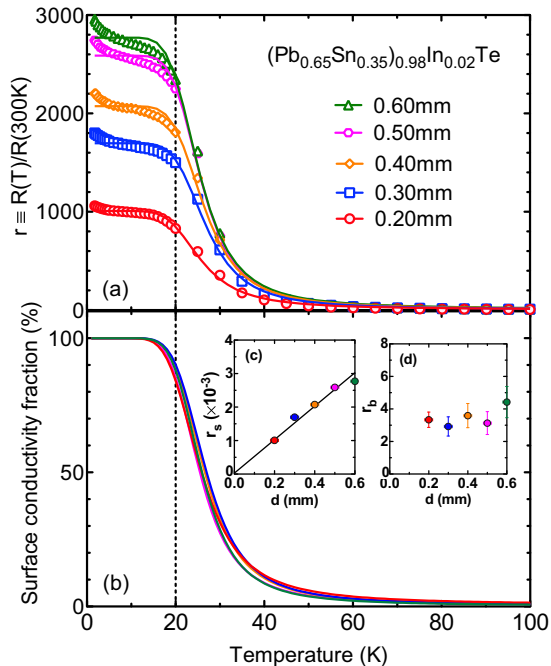


FIG. 4. (Color online) (a) Resistance normalized to its room-temperature value for several thicknesses of $(\text{Pb}_{0.65}\text{Sn}_{0.35})_{0.98}\text{In}_{0.02}\text{Te}$. Lines are fits as described in the text. Results for fitting parameters r_s and r_b are shown in panels (c) and (d), respectively. (b) Fraction of conductivity due to surface states calculated from the fit parameters.

VI. HALL EFFECT AND MAGNETORESISTANCE MEASUREMENTS

As another test, the Hall effect and zero-field resistivity were measured on a $x = 0.35$ and $y = 0.02$ crystal using a QD Physical Property Measurement System. From those measurements, we obtained the carrier density n and mobility μ shown in Figs. 5(a) and 5(b), respectively. The carrier density drops rapidly upon cooling, falling below $10^{14}/\text{cm}^3$ at 5 K, while the mobility rises rapidly below 20 K, eventually surpassing $2000 \text{ cm}^2 \text{ V}^{-1} \text{ s}^{-1}$, consistent with metallic conduction by surface states and negligible bulk contribution at low temperature.

As can be seen in Fig. 2, and as confirmed by ARPES (Fig. 3), the surface conduction channel exists and dominates the low-temperature transport on both topological and trivial sides of the phase diagram. Therefore, we perform the final test of the topological character of the surface states with magnetoresistance measurements [27]. The symmetry-protected coupling of spin and momentum for surface states makes them immune to weak localization effects. Application of a transverse magnetic field violates the relevant symmetries [28], thus removing the topological protection and leading to a field-induced decrease in conductance. Combining the longitudinal and transverse resistivity data, we have evaluated the field-dependent longitudinal conductivity. Results at 5 K and 20 K are plotted in Figs. 5(c) and 5(d), respectively.

For a quantitative analysis, we fit the data with the theoretical formula for weak antilocalization (WAL) [29],

$$\Delta G = \frac{\alpha e^2}{\pi h} \left[\ln(B_\phi/B) - \psi\left(\frac{1}{2} + B_\phi/B\right) \right], \quad (2)$$

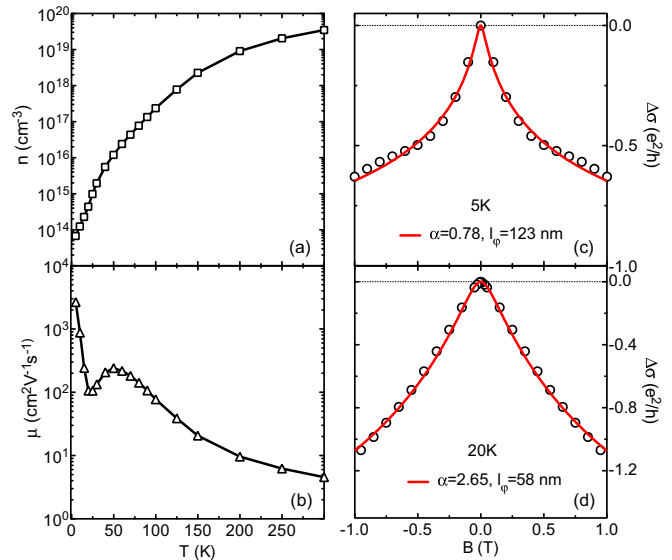


FIG. 5. (Color online) Characterizations of the $(\text{Pb}_{0.65}\text{Sn}_{0.35})_{0.98}\text{In}_{0.02}\text{Te}$ sample. (a) Carrier density, obtained from Hall effect measurements, and (b) carrier mobility vs T ; lines are guides to the eye. (c) Change in magnetoconductivity with the field at 5 K and (d) 20 K. Red lines represent fits to the WAL formula, Eq. (2), as discussed in the text. For the initial magnetoresistance data used to obtain $\sigma(B)$, the measurements were performed after a significant waiting time (5 days at 5 K, 2 days at 20 K) due to slow relaxation in the resistance [22].

where ψ is the digamma function and α is a number equal to $1/2$ times the number of conduction channels; $B_\phi = \Phi_0/(8\pi l_\phi^2)$, with $\Phi_0 = h/e$ and l_ϕ being the electronic phase coherence length. For our system, one expects four Dirac cones crossing the Fermi surface [30,31], which would give $\alpha = 2$. The fit to the 5-K data yields $\alpha = 0.78$ and $l_\phi = 123 \text{ nm}$; at 20 K, the fit gives $\alpha = 2.65$ and $l_\phi = 58 \text{ nm}$. The reduction in coherence length with temperature is consistent with the drop in mobility. The magnitude of α is qualitatively consistent with expectations, though the temperature dependence is unexpected. Note that for the $x = 0.5$ and $y = 0.06$ sample, the magnetoresistance was measured at 5 K; a fit of the WAL formula to the data yields $l_\phi = 100 \text{ nm}$ and $\alpha = 2.25$, close to the expected $\alpha = 2$.

VII. CONCLUSIONS

In conclusion, we have shown that crystals of In-doped $\text{Pb}_{1-x}\text{Sn}_x\text{Te}$ with $x \sim 0.3$ have true bulk-insulating resistivity, and we have presented evidence for conductivity by nontrivial topological surface states below 20 K for $x = 0.35$. This allows one to exploit the unusual properties of the surface states in transport measurements without the need to apply a bias voltage to the surface. There is also strong interest in inducing topological superconductivity at surfaces or interfaces [2], and we note that there are exciting possibilities to create interfaces between the present topological insulators and superconductors of closely related alloys [20,32], such as In-doped SnTe and $\text{Pb}_{0.5}\text{Sn}_{0.5}\text{Te}$.

ACKNOWLEDGMENTS

We thank W.-G. Yin for discussions. Work at Brookhaven National Laboratory is supported by the Office of Basic Energy Sciences, Division of Materials Sciences and Engineering, US Department of Energy, under Contract No. DE-SC00112704;

use of facilities at the Center for Functional Nanomaterials and at the NSLS was supported by the Office of Basic Energy Sciences, Division of Scientific User Facilities. I.P. is supported by the Army Research Office MURI on Topological Insulators, Grant No. W911NF-12-1-0461.

-
- [1] M. Z. Hasan and C. L. Kane, Colloquium: Topological insulators, *Rev. Mod. Phys.* **82**, 3045 (2010).
- [2] X.-L. Qi and S.-C. Zhang, Topological insulators and superconductors, *Rev. Mod. Phys.* **83**, 1057 (2011).
- [3] H. Weng, X. Dai, and Zh. Fang, Exploration and prediction of topological electronic materials based on first-principles calculations, *MRS Bull.* **39**, 849 (2014).
- [4] L. Fu, Topological crystalline insulators, *Phys. Rev. Lett.* **106**, 106802 (2011).
- [5] T. H. Hsieh, H. Lin, J. Liu, W. Duan, A. Bansil, and L. Fu, Topological crystalline insulators in the SnTe material class, *Nat. Commun.* **3**, 982 (2012).
- [6] Y. Tanaka, Z. Ren, T. Sato, K. Nakayama, S. Souma, T. Takahashi, K. Segawa, and Y. Ando, Experimental realization of a topological crystalline insulator in SnTe, *Nat. Phys.* **8**, 800 (2012).
- [7] P. Dziawa, B. J. Kowalski, K. Dybko, R. Buczko, A. Szczerbakow, M. Szot, E. Łusakowska, T. Balasubramanian, B. M. Wojek, M. H. Berntsen, O. Tjernberg, and T. Story, Topological crystalline insulator states in $\text{Pb}_{1-x}\text{Sn}_x\text{Se}$, *Nat. Mater.* **11**, 1023 (2012).
- [8] S.-Y. Xu, C. Liu, N. Alidoust, M. Neupane, D. Qian, I. Belopolski, J. D. Denlinger, Y. J. Wang, H. Lin, L. A. Wray, G. Landolt, B. Slomski, J. H. Dil, A. Marcinkova, E. Morosan, Q. Gibson, R. Sankar, F. C. Chou, R. J. Cava, A. Bansil, and M. Z. Hasan, Observation of a topological crystalline insulator phase and topological phase transition in $\text{Pb}_{1-x}\text{Sn}_x\text{Te}$, *Nat. Commun.* **3**, 1192 (2012).
- [9] C. Yan, J. Liu, Y. Zang, J. Wang, Z. Wang, P. Wang, Z.-D. Zhang, L. Wang, X. Ma, S. Ji, K. He, L. Fu, W. Duan, Q.-K. Xue, and X. Chen, Experimental observation of dirac-like surface states and topological phase transition in $\text{Pb}_{1-x}\text{Sn}_x\text{Te}$ (111) films, *Phys. Rev. Lett.* **112**, 186801 (2014).
- [10] H. Peng, K. Lai, D. Kong, S. Meister, Y. Chen, X.-L. Qi, S.-C. Zhang, Z.-X. Shen, and Y. Cui, Aharonov-Bohm interference in topological insulator nanoribbons, *Nat. Mater.* **9**, 225 (2010).
- [11] J. G. Analytis, R. D. McDonald, S. C. Riggs, J.-H. Chu, G. S. Boebinger, and Ian R. Fisher, Two-dimensional surface state in the quantum limit of a topological insulator, *Nat. Phys.* **6**, 960 (2010).
- [12] J. Xiong, Y. Luo, Y. Khoo, S. Jia, R. J. Cava, and N. P. Ong, High-field Shubnikov-de Haas oscillations in the topological insulator $\text{Bi}_2\text{Te}_2\text{Se}$, *Phys. Rev. B* **86**, 045314 (2012).
- [13] Z. Ren, A. A. Taskin, S. Sasaki, K. Segawa, and Y. Ando, Optimizing $\text{Bi}_{2-x}\text{Sb}_x\text{Te}_{3-y}\text{Se}_y$ solid solutions to approach the intrinsic topological insulator regime, *Phys. Rev. B* **84**, 165311 (2011).
- [14] Y. Pan, D. Wu, J. R. Angevaere, H. Luigjes, E. Frantzeskakis, N. de Jong, E. van Heumen, T. V. Bay, B. Zwartsenberg, Y. K. Huang, M. Snelder, A. Brinkman, M. S. Golden, and A. de Visser, Low carrier concentration crystals of the topological insulator $\text{Bi}_{2-x}\text{Sb}_x\text{Te}_{3-y}\text{Se}_y$: A magnetotransport study, *New J. Phys.* **16**, 123035 (2014).
- [15] B. Skinner, T. Chen, and B. I. Shklovskii, Why is the bulk resistivity of topological insulators so small? *Phys. Rev. Lett.* **109**, 176801 (2012).
- [16] B. A. Akimov, N. B. Brandt, L. I. Ryabova, V. V. Sokovishin, and S. M. Chudinov, Band edge motion in quantizing magnetic field and nonequilibrium states in $\text{Pb}_{1-x}\text{Sn}_x\text{Te}$ alloys doped with In, *J. Low Temp. Phys.* **51**, 9 (1983).
- [17] J. O. Dimmock, I. Melngailis, and A. J. Strauss, Band structure and laser action in $\text{Pb}_x\text{Sn}_{1-x}\text{Te}$, *Phys. Rev. Lett.* **16**, 1193 (1966).
- [18] X. Gao and M. S. Daw, Investigation of band inversion in (Pb,Sn)Te alloys using *ab initio* calculations, *Phys. Rev. B* **77**, 033103 (2008).
- [19] Y. Tanaka, T. Sato, K. Nakayama, S. Souma, T. Takahashi, Z. Ren, M. Novak, K. Segawa, and Y. Ando, Tunability of the k -space location of the dirac cones in the topological crystalline insulator $\text{Pb}_{1-x}\text{Sn}_x\text{Te}$, *Phys. Rev. B* **87**, 155105 (2013).
- [20] R. D. Zhong, J. A. Schneeloch, T. S. Liu, F. E. Camino, J. M. Tranquada, and G. D. Gu, Superconductivity induced by In substitution into the topological crystalline insulator $\text{Pb}_{0.5}\text{Sn}_{0.5}\text{Te}$, *Phys. Rev. B* **90**, 020505 (2014).
- [21] D. V. Shamshur, R. V. Parfen'ev, A. V. Chernyaev, and S. A. Némov, Low-temperature electrical conductivity and the superconductor-insulator transition induced by indium impurity states in $(\text{Pb}_{0.5}\text{Sn}_{0.5})_{1-x}\text{In}_x\text{Te}$ solid solutions, *Phys. Solid State* **52**, 1815 (2010).
- [22] Y. I. Ravich and S. A. Némov, Hopping conduction via strongly localized impurity states of indium in PbTe and its solid solutions, *Semiconductors* **36**, 1 (2002).
- [23] A. Strauss, Inversion of conduction and valence bands in $\text{Pb}_{1-x}\text{Sn}_x\text{Se}$ alloys, *Phys. Rev.* **157**, 608 (1967).
- [24] A. A. Taskin, Z. Ren, S. Sasaki, K. Segawa, and Y. Ando, Observation of Dirac holes and electrons in a topological insulator, *Phys. Rev. Lett.* **107**, 016801 (2011).
- [25] D.-J. Kim, J. Xia, and Z. Fisk, Topological surface state in the Kondo insulator samarium hexaboride, *Nat. Mater.* **13**, 466 (2014).
- [26] P. Syers, D. Kim, M. S. Fuhrer, and J. Paglione, Tuning bulk and surface conduction in the proposed topological Kondo insulator SmB_6 , *Phys. Rev. Lett.* **114**, 096601 (2015).
- [27] N. Bansal, Y. S. Kim, M. Brahlek, E. Edrey, and S. Oh, Thickness-independent transport channels in topological insulator Bi_2Se_3 thin films, *Phys. Rev. Lett.* **109**, 116804 (2012).

- [28] M. Serbyn and L. Fu, Symmetry breaking and Landau quantization in topological crystalline insulators, *Phys. Rev. B* **90**, 035402 (2014).
- [29] S. Hikami, A. I. Larkin, and Y. Nagaoka, Spin-orbit interaction and magnetoresistance in the two-dimensional random system, *Prog. Theor. Phys.* **63**, 707 (1980).
- [30] J. Liu, W. Duan, and L. Fu, Two types of surface states in topological crystalline insulators, *Phys. Rev. B* **88**, 241303 (2013).
- [31] B. A. Assaf, F. Katmis, P. Wei, B. Satpati, Z. Zhang, S. P. Bennett, V. G. Harris, J. S. Moodera, and D. Heiman, Quantum coherent transport in SnTe topological crystalline insulator thin films, *Appl. Phys. Lett.* **105**, 102108 (2014).
- [32] R. D. Zhong, J. A. Schneeloch, X. Y. Shi, Z. J. Xu, C. Zhang, J. M. Tranquada, Q. Li, and G. D. Gu, Optimizing the superconducting transition temperature and upper critical field of $\text{Sn}_{1-x}\text{In}_x\text{Te}$, *Phys. Rev. B* **88**, 020505 (2013).